HAL open science

HDL Simulation of a Thermal Accelerometer for System Design

Aboubacar Chaehoi, Laurent Latorre, Olivier Leman, Frédérick Mailly, Pascal Nouet

To cite this version:

Aboubacar Chaehoi, Laurent Latorre, Olivier Leman, Frédérick Mailly, Pascal Nouet. HDL Simulation of a Thermal Accelerometer for System Design. XX EUROSENSORS, Sep 2006, Göteborg (Sweden). lirmm-00102170

HAL Id: lirmm-00102170

https://hal-lirmm.ccsd.cnrs.fr/lirmm-00102170v1

Submitted on 29 Sep 2006

HAL is a multi-disciplinary open access archive for the deposit and dissemination of scientific research documents, whether they are published or not. The documents may come from teaching and research institutions in France or abroad, or from public or private research centers.

L'archive ouverte pluridisciplinaire **HAL**, est destinée au dépôt et à la diffusion de documents scientifiques de niveau recherche, publiés ou non, émanant des établissements d'enseignement et de recherche français ou étrangers, des laboratoires publics ou privés.

HDL SIMULATION OF A THERMAL ACCELEROMETER FOR SYSTEM DESIGN

O. Leman, A. Chaehoi, F. Mailly, L. Latorre* and P. Nouet
Laboratoire d'Informatique de Robotique et de Microélectronique de Montpellier
UMR 5506 – CNRS / University Montpellier II, 161 rue Ada, 34392,
Montpellier - France

*Corresponding author: Laurent Latorre, Tel: +33 467 418 665, email: latorre@lirmm.fr

Abstract: This study concerns the integration of convective accelerometers on CMOS. The design approach is based on an HDL modeling of the sensing cell. The development of a monolithic system is then illustrated using multi-domain simulations within the microelectronic design environment. For illustration, the sensor equivalent input noise (i.e. the resolution) is then computed for various readout circuitry configurations.

Keywords: MEMS, accelerometer, HDL modeling

INTRODUCTION

Convective accelerometers are quite different from their seismic-mass-based equivalents. Their working principle relies on the heating of a small volume of gas, air at atmospheric pressure in our case, which is disturbed by an applied acceleration. As a result, a temperature gradient appears in the gas volume, which can be measured by means of temperature sensors. Such structures have been investigated for decades and reported on silicon [1-4].
This work addresses the implementation of this sensing principle on standard CMOS technology. This monolithic approach allows batch production and dramatic costs reductions over hybrid sensors which use MEMS and signal conditioning on several dedicated dies. The aim is to provide microelectronics engineers with MEMS IPs, similar in use to analog cells coming from design kit libraries, which can be tailored to the desired dimensions, integrated among the signal conditioning electronics, and finally simulated within the design environment.

Our modeling approach relies on the use of heat transfer fundamentals and empirical parameters, provided by previous FEM simulations and characterizations of physical test vehicles [5, 6]. Those complementary methods have led to a compact model, ready for HDL integration and system optimization.

DEVICE UNDER STUDY

The accelerometer is composed of three suspended bridges, composed of the CMOS back-end layers (oxide, polysilicon, aluminum, and nitride). Polysilicon is used to implement resistors, for both eating (Rh) and sensing (Rd_1, Rd_2) purposes (figure 1a).
The heater R_H is supplied by an electrical current in order to create a temperature gradient in the top and bottom cavities (figure 1b): the temperature is then maximum at the heater location and minimum at the cavities boundaries. In absence of acceleration, the detectors measure the same temperature for symmetry reason. As a result of an acceleration, the temperature gradient deforms and a temperature difference can be measured across the detectors. Because the resistors are temperature-dependent, the signal is converted into a voltage by means of a Wheatstone bridge.

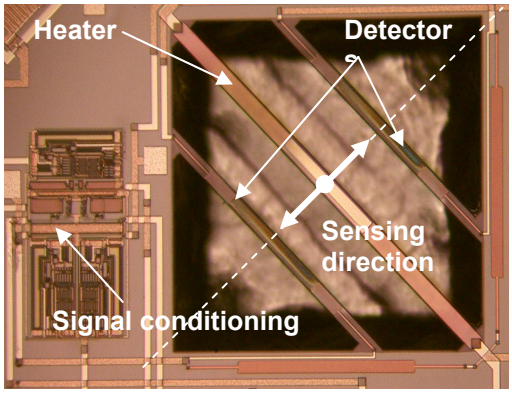

(a)

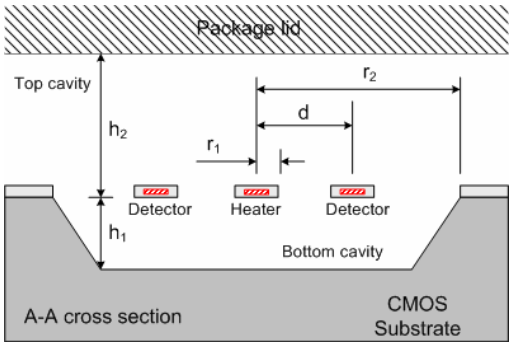

(b)

Figure 1. Picture of the sensor (a) and cross section of the sensor with dimension parameters (b).

In order to compare experimental results with FEM simulation and to build an HDL model of the sensor, two prototype versions (A and B) have been designed, fabricated and characterized. Table 1 summarizes their physical parameters.

	A	B
r_1	20 µm	20 µm
r_2	570 µm	340 µm
D	200 µm	125 µm
Rh	720 Ω	350 Ω
Rd_1, Rd_2	50 kΩ	50 kΩ
h_1	≈ 300 µm	
h_2	≈ 1 mm	

Table 1 . Physical parameters of the two prototypes

HDL MODEL OF THE SENSOR

The HDL model of the sensor is represented on the figure 2 and some details are given in [7]. Section 1 models the average temperature of the heating bridge:

$$\Delta T_H = T_H - T_A = R_{th} \times P_H$$

where T_H and T_A (K) are respectively the average heater temperature and ambient temperature, R_{th} ($K.W^{-1}$) is the equivalent thermal resistance of the beam and P_H (W) is the joule power dissipated in the heater resistance. Note that the value of the heater resistance also increases linearly with its temperature.

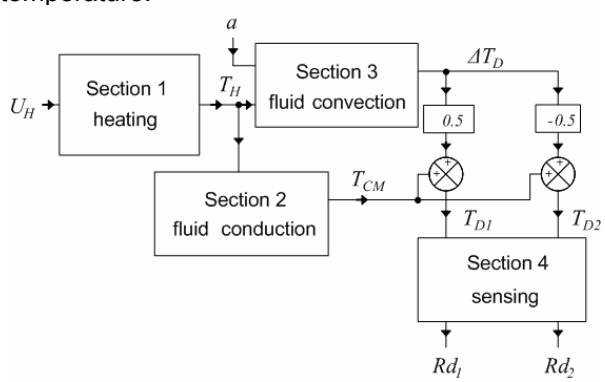

Figure 2. Functional bloc representation of the model.

Heat transfer in the air, from the heater to the detectors, is then separated into two functional blocs. The first one (section 2) describes the conduction heat transfer, which was shown to be responsible of the common mode temperature on detectors. This model is based on a cylindrical geometry approximation and the common mode temperature at a distance *r* from the heater is ruled by:

$$T + \gamma \frac{T^2}{2} = \frac{\left[(T_H - T_A) + \frac{\gamma}{2}\left(T_H^{\,2} - T_A^{\,2}\right) \right]}{\ln\left(\frac{r_2}{r_1}\right)} \cdot \ln\left(\frac{r}{r_1}\right) + T_H + \gamma \frac{T_H^{\,2}}{2} \qquad (1)$$

The second one (section 3) expresses convective transfer from which depends the output signal. The temperature profile established in section 2 deforms, producing a temperature difference across the detectors ΔT_D. This temperature difference has been found to be proportional to the Grashof number [1-6]:

$$\Delta T_D = \frac{S.Gr}{1+\tau p} = S.\frac{a\beta\rho^2 (Ts - Ta) l^3}{\mu^2} \frac{1}{1+\tau p} \qquad (2)$$

with *S* (K) a fitting coefficient (extracted from FEM analysis and experimental results) which represents the system sensitivity, *a* ($m.s^{-2}$) the acceleration, *ρ* ($kg.m^{-3}$) the gas density , *β* (K^{-1}) the gas coefficient of expansion, *μ* ($kg.m^{-1}.s^{-1}$) the gas viscosity, *l* (m) a linear dimension related to the cavity volume and geometry and *τ* (s) the time constant of the fluid.

Finally, section 4 implements detectors transfer function taking into account the temperature sensitivity of the polysilicon (TCR) and the thermal time constant of the bridges (τ_D):

$$Rd_i = Rd_{i,nom}\left(1 + TCR\left(T_{CM} \pm \frac{1}{2}\Delta T_D\right)\frac{1}{1+\tau_D p}\right) \qquad (3)$$

Then, detectors variations are converted by a Wheatstone bridge and a thermal noise spectral density is also added:

$$V_{n,i}^{\,2}(f) = 4kT_{D,i}Rd_i \qquad (4)$$

SYSTEM LEVEL DESIGN

This HDL model is used to develop on-chip circuitry in order to raise overall system performance. The white noise level at the output of the Wheatstone bridge is computed first and considered as a noise floor reference (intrinsic noise). The simulation takes into account the common mode temperature of the detectors.

Three readout interfaces have been compared using multi-domain simulations within Cadence®. The first interface is a simple instrumentation amplifier ("amplifier 1") of gain 1000 (see figure 3-a) which was implemented on our first prototype [5-6]. Figure 4 shows that the input noise spectral density is then at least one order of magnitude greater than the intrinsic noise in the sensor bandwidth (from DC to 10Hz). This is due to 1/f noise of the CMOS transistors. Assuming a low-pass filtering of the output voltage from DC to 100Hz, the RMS noise voltage would be 2.33 μV_{RMS}. Taking into account the sensitivity of our first prototype (375 µV/g without amplification [5, 6]), the equivalent noise acceleration would be 6 mg.

For the second case (amplifier 2) a dedicated low-noise preamplifier of gain 10 has been customized

and placed right after the Wheatstone bridge (see figure 3-b). The CMOS transistors of the differential pair were dimensioned (W = 400µm, L = 6µm) to reduce their 1/f noise and the instrumentation amplifier gain was set to 100. Figure 4 shows that the noise density is then reduced in the sensor bandwidth and 100Hz low-pass filtering would lead to a noise voltage of 549 nV_{RMS} and to a resolution improvement of the sensor by a factor 4.

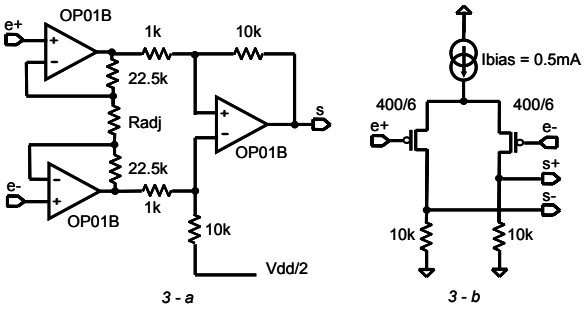

Figure 3. Amplifier Schematic

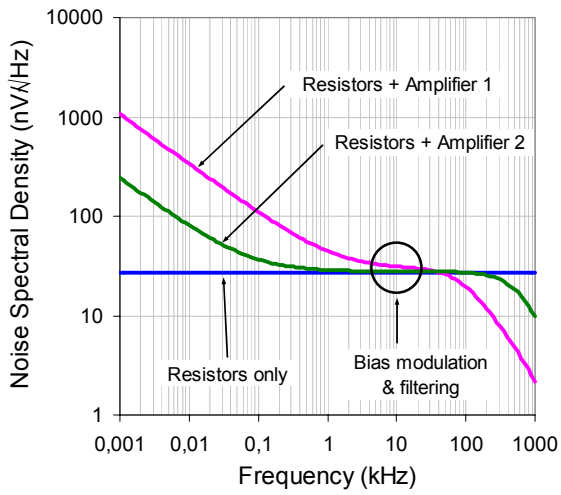

Figure 4. Equivalent input noise spectral density.

Amplifier	f_M (kHz)	e_{noise} (nV.Hz$^{-1/2}$)
1	1	45.5
1	5	33.6
1	10	31.7
2	1	26.9
2	5	26.2
2	10	26.1

Table 2. Equivalent input noise spectral density for different bias modulation frequencies.

A modulation of the Wheatstone bridge bias at high frequency (i.e. before the amplifier cutoff frequency) can improve the sensor resolution by reducing the output noise close to the intrinsic noise level of the sensor (26 nV.Hz$^{-1/2}$). Table 2 gives the average RMS noise spectral density around different modulation frequencies f_M (1, 5 and 10 kHz). It shows that a band-pass filter has to be used to improve the sensor resolution.

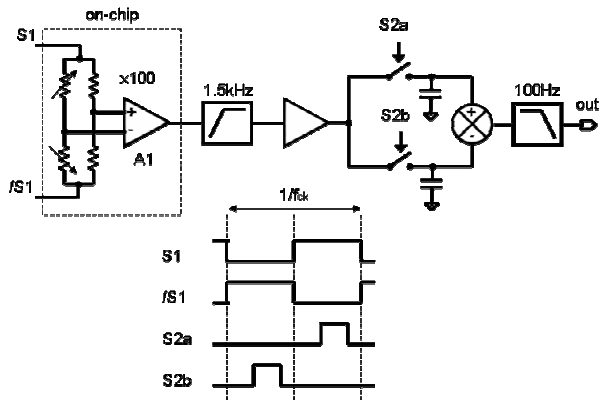

Figure 5. Electronic architecture based on a chopper-stabilized amplifier with a track-and-hold signal demodulator

Another solution is to use a chopper-stabilized amplifier with a track-and-hold signal demodulator. Electronic architecture is presented on figure 5. As a symmetrical square wave biasing is used, the sensor sensitivity is now twice higher. A high-pass filter (f_c = 1.5kHz) is used to eliminate the flicker noise of the on-chip amplifier and to reach the intrinsic noise of the resistors. Considering an input white noise spectral density V_{in} = 26nV.Hz$^{-1/2}$ from DC to the amplifier cut-off frequency (f_c), the output noise voltage V_{out} of the track-and-hold demodulator is given by [8, 9]:

$$\left(\frac{V_{out}^2}{V_{in}^2}\right)_{f<f_{ck}/2} \approx d^2\left[1+2\sum_{n=1}^{h} sinc^2(nd)\right]+(1-d)^2(1+2h) \quad (5)$$

where, f_{ck} is the clock frequency of the demodulator, d is the duty cycle of the track operation and h is the closest integer to the f_c/f_{ck} ratio.
With f_{ck} = 20kHz, f_c = 100kHz, and d=0.4, this architecture should permit to reach an output noise only twice higher than the intrinsic noise of the sensor.

Obviously, the intrinsic noise of the sensor and its resolution would also be improved by reducing the nominal resistance of the detectors.

EXPERIMENTAL RESULTS

This section presents experimental results obtained with the two prototypes. To reduce the supply noise density and 50Hz parasitic signals, a battery is used as the power supply. The heater power is adjusted to obtain the same heater temperature on both sensors. First measurements have been made using 5V (dc) to bias the Wheatstone bridge and to

supply the on-chip amplifier (amplifier 1) and an external additional amplifier. As the sensor bandwidth is about 15Hz, the output signal is low-pass filtered at 100Hz to remove the high frequency noise. Table 3 presents the results obtained with both sensors. These results are presented in terms of equivalent input noise voltage and input sensitivity. It takes into account the electronic gain (amplifier 1 + external). The noise voltages equal $3.54\mu V_{RMS}$ and $3.85\mu V_{RMS}$ for the sensors A and B respectively, very close to the $2.33\mu V_{RMS}$ calculated by simulation. Since the sensitivity of the sensor A is higher, its noise equivalent acceleration (NEA) is lower.

	Sensor A		Sensor B	
P_{heater} (mW)	27		20	
T_{heater} (°C)	325		325	
Wheatstone bridge bias	DC	20kHz square wave	DC	20kHz square wave
Sensitivity ($\mu V.g^{-1}$)	200	379	69	138
e_{noise} ($nV_{RMS}.Hz^{-1/2}$)	354	218	385	215
NEA ($mg.Hz^{-1/2}$)	1.8	0.6	5.6	1.55

Table 3. Experimental results

The chopper-stabilized amplifier with the track-and-hold signal demodulator (figure 5) has been also tested. As expected, sensitivities are twice higher on both sensors. Noise voltage and noise equivalent acceleration have been also improved.

CONCLUSION

This paper addresses the design of CMOS convective accelerometers. An HDL model is proposed for a three-bridges sensor. This model is used for system level simulation in Cadence®. As an illustration of system level simulations, three readout circuitry configurations are compared, from the simple instrument amplifier to a complete synchronous detection scheme. It is shown that using a bias modulation and subsequent filtering, the noise of the electronics can be neglected compared to the intrinsic noise of the sensor itself. This result is confirmed by experimental results obtained from two prototypes.

REFERENCES

1. A.M. Leung, J. Jones, E. Czyzewska, J. Chen, B. Woods, Micromachined accelerometer based on convection heat transfer, *proc. IEEE MEMS'98*, Heidelberg, Germany, 25-29 Jan. 1998, pp. 627–630.
2. V. Milanovic, E. Bowen, M. E. Zaghloul, N. H. Tea, J. S. Suehle, B. Payne, and M. Gaitan, Micromachined convective accelerometers in standard integrated circuits technology, Appl. Phys. Lett. 76 (4) (2000), pp. 508-510.
3. F. Mailly, A. Giani, A. Martinez, R. Bonnot, P. Temple-Boyer and A. Boyer, Micromachined thermal accelerometer, Sens. Actuators A 103 (3) (2003), pp. 359-363.
4. X.B. Luo, Y.J. Yang, F. Zheng, Z.X. Li and Z.Y. Guo, An optimized micromachined convective accelerometer with no proof mass, J. Michromech. Microeng. 11 (2001), pp. 504-508.
5. A. Chaehoi, L. Latorre, F. Mailly, P. Nouet, Experimental and finite-element study of convective accelerometer on CMOS, proc. EUROSENSORS'05, Barcelona, Spain, Sept. 11-14, 2005.
6. A. Chaehoi, F. Mailly, L. Latorre, P. Nouet, Experimental and finite-element study of convective accelerometer on CMOS, extended paper of Eurosensors'05, to be published in Sens. Actuators.
7. O. Leman, A. Chaehoi, F. Mailly, L. Latorre, P. Nouet, Modeling of a CMOS Convective Accelerometer for HDL Integration, proc. ESSDERC 2006, Montreux, Switzerland, Sept. 18-22, 2006.
8. J. H. Fischer, Noise sources and calculation techniques for switched capacitor filters, IEEE Journal of Solid-state Circuits, Vol. SC-17, no. 4 (1982), pp.742-752.
9. A Billoti, G. Monreal, Chopper-stabilized amplifiers with a track-and-hold signal demodulator, technical paper STP 99-1, Allegro MicroSystems.